Experimental and kinetic modeling studies of methanol synthesis from CO<inf>2</inf> hydrogenation using In<inf>2</inf>O<inf>3</inf> catalyst

Chemical Engineering Journal 416 (2021) 129120

Contents lists available at ScienceDirect

Chemical Engineering Journal

journal homepage: www.elsevier.com/locate/cej

Experimental and kinetic modeling studies of methanol synthesis from CO_2 hydrogenation using In_2O_3 catalyst

Sreetama Ghosh, Joby Sebastian, Louise Olsson, Derek Creaser *

Competence Centre for Catalysis, Chemical Engineering, Chalmers University of Technology, SE - 41296 Gothenburg, Sweden

ARTICLE INFO

Keywords:
Carbon capture and utilization (CCU)
Methanol synthesis
CO_2 hydrogenation, Indium oxide
Kinetic model

ABSTRACT

Catalytic hydrogenation of CO_2 to methanol has gained considerable interest for its significant role in CO_2 utilization using heterogeneous catalysts. This study is the first to propose a kinetic model based on Langmuir-Hinshelwood-Hougen-Watson (LHHW) mechanism for CO_2 hydrogenation to methanol over a highly effective indium oxide (In_2O_3) catalyst. The work focuses on different reaction conditions mainly revolving around the variation of operating temperature, total reactor pressure, H_2/CO_2 molar feed ratio and weight hourly space velocity (WHSV) of the system. The experimental data were modeled using a competitive single-site kinetic model based on LHHW rate equations. A parameter optimization procedure was undertaken to determine the kinetic parameters of the developed rate equations. The model predicts that when the methanol synthesis reaction becomes equilibrium limited, the progress of the RWGS reaction forces the methanol yield to decrease due to the reversal of the methanol synthesis reaction. A mixture of CO_2 and H_2 has been used as the reactor feed in all the cases. Significantly w.r.t. the CO_2 partial pressure, the reaction rate for methanol synthesis initially increased and then slightly decreased indicating a varying order. The single-site model accurately predicted the trends in the experimental data which would enable the development of reliable reactor and process designs.

1. Introduction

Growing energy demand, depletion of fossil fuel reserves and increasing atmospheric carbon dioxide (CO_2) concentrations call for the usage of renewable energy resources such as solar, wind and biomass. However, the widespread utilization of these sustainable energy sources is currently limited by their intermittent and fluctuating nature. Carbon capture and utilization (CCU) have been proposed as the ultimate way to manage global CO_2 levels. However, CO_2 is a thermally stable and chemically inert molecule with a standard enthalpy of formation of -396.0 kJ mol^{-1} and hence a large energy input is necessary for its chemical transformation [1,2]. In this context, the catalytic conversion of CO_2 to value-added chemicals and fuels by using energy-rich hydrogen obtained sustainably from biomass reforming and water splitting is a promising solution for future energy demand. Methanol synthesis by catalytic reduction of CO_2 is highly attractive as the produced methanol can be a fuel itself or used for the well-known methanol-to-hydrocarbon (MTH) reaction process to produce hydrocarbon fuels. Commercially, methanol is produced from a mixture of $CO/CO_2/H_2$ (synthesis gas containing ca. 3 vol% CO_2) [3] using a $Cu/ZnO/Al_2O_3$ catalyst at typical reaction conditions of 230–280 °C and 50–120 atm pressure [2,4]. Several experimental studies reveal that CO_2 in the synthesis gas is an important carbon source for methanol synthesis [5].

Catalytic hydrogenation of CO_2 mainly involves the following reversible reactions:[6]

$$CO_2 + 3H_2 \rightleftarrows CH_3OH + H_2O \quad \Delta G(25^{\circ}C) = -0.47\,kJ\,mol^{-1} \tag{1}$$

$$CO_2 + H_2 \rightleftarrows CO + H_2O \quad \Delta G(25^{\circ}C) = 23.4\,kJ\,mol^{-1} \tag{2}$$

$$CO_2 + 4H_2 \rightleftarrows CH_4 + 2H_2O \quad \Delta G(25^{\circ}C) = -130.8\,kJ\,mol^{-1} \tag{3}$$

Eq. (1) corresponds to the methanol synthesis reaction, eq. (2) is the Reverse Water-Gas Shift (RWGS) reaction and eq. (3) stands for the CO_2 methanation reaction (also called the Sabatier reaction). Thermodynamically, eq. (3) is the most thermodynamically favored with ΔG (25 °C) = -130.8 kJ mol^{-1} [7]. The desired reaction is, of course, methanol synthesis reaction but the RWGS reaction producing CO and methanation reaction producing CH_4, are considered as significant side reactions and hence these byproducts have also been considered in this study. The RWGS reaction is an endothermic reaction facilitated by high

* Corresponding author.
E-mail address: derek.creaser@chalmers.se (D. Creaser).

https://doi.org/10.1016/j.cej.2021.129120
Received 17 November 2020; Received in revised form 31 January 2021; Accepted 20 February 2021
Available online 27 February 2021

temperatures [2]. Reactions involving eq. (1) and eq. (3) are exothermic, and particularly for the less thermodynamically favorable methanol synthesis, a tradeoff temperature is required to maximize the CO_2 conversion to methanol [8].

Kinetic modeling finds wide applications in biomass utilization [9–11]. Among the different catalytic materials investigated so far for CO_2 hydrogenation to methanol, Cu-based catalysts have attracted much attention due to the high intrinsic activity of Cu [4,12–16]. Therefore, most of the kinetic models for methanol synthesis are centered on Cu-based catalysts. A model obtained for a Cu/ZnO catalyst presented by Klier *et al.* showed that the rate of methanol conversion significantly increased with the addition of CO_2 along with CO and H_2 in the feed [17]. A Langmuir-Hinshelwood-Hougen-Watson (LHHW) rate expression was applied by Villa *et al.* for a commercial $Cu/ZnO/Al_2O_3$ catalyst both for methanol synthesis as well as the RWGS reaction. The mechanism was based on the non-dissociative adsorption of CO and H_2 [18]. These kinetic studies were based on a single-site model. Later, a dual-site model based on an LHHW rate expression was proposed by Graaf *et al.* by considering dissociative adsorption of H_2 over $Cu/ZnO/Al_2O_3$. The feed gas was a mixture of $CO/CO_2/H_2$ gas. On one site CO and CO_2 could competitively adsorb, while the other site was dedicated to the competitive adsorption of H_2 and H_2O. The adsorption of methanol was assumed to be negligible on these sites [19–21]. In Cu/ZnO catalysts, adsorption and dissociation of H_2 are considered to occur on the Cu-sites, whereas, ZnO is responsible for CO_2 adsorption as bicarbonate species [22]. The model of Graaf *et al.* has later been validated and extended for use for a wider range of reaction conditions in several other kinetic modeling studies focused on the hydrogenation of CO_2 to methanol [8,23–27]. However, the Cu-based catalysts have certain limitations. For instance, the industrial $Cu/ZnO/Al_2O_3$ catalyst is less selective towards methanol directly from CO_2 owing to its high activity towards the RWGS reaction when a mixed syngas ($CO/CO_2/H_2$) is used as feed and it is also less stable due to the deactivating effect of the additional H_2O produced as a byproduct of the RWGS reaction [3,28].

Recent studies have shown that In_2O_3 based catalysts are highly selective for methanol from CO_2 *via* its direct hydrogenation [28,29]. The high selectivity of the catalyst was attributed to its ability to inhibit the RWGS reaction. Based on density functional theory (DFT) studies on a model (1 1 0) surface of In_2O_3, methanol formation proceeds through the surface formate (HCOO) species[30], where the surface oxygen vacancies act as active sites for CO_2 activation and hydrogenation to form methanol [31]. A microkinetic analysis was performed by Frei *et al.* for In_2O_3 using Arrhenius and reaction order plots [3]. In addition, a mechanistic model with corresponding energy levels was developed based on DFT simulations over the (1 1 1) plane of In_2O_3 [3].

However, to the best of our knowledge, there are no results of kinetic models based on the LHHW mechanism published that describe CO_2 hydrogenation to methanol over In_2O_3, which is the objective of the current work. Herein, a fundamental understanding of the kinetics of methanol (CH_3OH) synthesis from CO_2 hydrogenation is studied over an unsupported In_2O_3 catalyst to develop an effective, robust and practical LHHW kinetic model. An understanding of the kinetic and thermodynamic coupling of the CO_2 hydrogenation to methanol and the RWGS reactions by a modeling technique is presented here. A comparative study between single-site and dual-site kinetic models is also performed to evaluate their consistencies with the experimental data. An isothermal fixed bed reactor was used to execute the catalytic reactions with a temperature ranging between 200 and 400 ℃, a total pressure between 20 and 40 bar, varying H_2:CO_2 molar feed ratios (2:1–6:1) and a range of WHSV (weight hourly space velocity) from 6000 to 16000 mL $g_{cat}^{-1}h^{-1}$. The developed set of optimized kinetic parameters from this model could enable the design of reactors for this catalytic system.

2. Experimental

2.1. Catalyst preparation

Indium hydroxide, $In(OH)_3$, was first synthesized by the standard precipitation method. An aqueous solution of Na_2CO_3 (10 g, Sigma Aldrich, ≥99.5%) was slowly added dropwise to the aqueous solution of Indium (III) nitrate hydrate (7.7 g, Sigma Aldrich, 99.99%) under magnetic stirring until the pH reached ~ 9.2. The resulting solution was aged for 1 h under continuous stirring and then filtered and washed profusely with deionized water. The sample was then collected and dried in a vacuum oven overnight at 60 ℃. The resultant white $In(OH)_3$ powder was then calcined by heating at a ramp rate of 2 ℃ min^{-1} and maintained at 300 ℃ for 3 h, to obtain crystalline In_2O_3 powder [32]. The In_2O_3 powder thus obtained was pressed, crushed and sieved to granules with a size range of 350 to 500 μm. As a diluent to ensure isothermal conditions in the reactor, these In_2O_3 granules were mixed with commercial SiO_2 granules of the same size range by mechanical shaking in a 2:1 mass ratio of In_2O_3 and SiO_2.

2.2. Catalyst characterization

The morphology of the catalyst was examined using Scanning electron microscopy (SEM) and Transmission electron microscopy (TEM). SEM analysis was performed using JEOL 7800F Prime and TEM was done using an FEI Titan 80–300 instrument having an accelerating voltage of 300 kV. The lattice spacing was measured using Gatan Digital Micrograph software. The crystalline nature of the sample was analyzed from the X-Ray diffraction (XRD) pattern that was obtained using a Bruker D8 X-ray Diffractometer with CuK_α ($\lambda = 1.54$ Å) radiation within a scanning angle of 2θ from 20 to 80°. The specific surface area and pore size distribution were measured from nitrogen physisorption isotherm analysis carried out using a Micromeritics Tristar 3000 surface area and porosity analyzer. The catalyst was degassed at 300 ℃ for 3 h under nitrogen flow before the analysis. The specific surface area was calculated using the Brunauer-Emmett-Teller (BET) equation and the pore size was estimated using the Barrett-Joyner-Halenda (BJH) equation. X-ray Photoelectron Spectroscopy (XPS) studies were performed using a PerkinElmer PHI 5000 VersaProbe III Scanning XPS Microprobe. The sample was irradiated with a monochromatic Al-Kα source with a binding energy of 1486.6 eV in a vacuum chamber. The data obtained were analyzed by using Multipack software and with CasaXPS.

2.3. Catalytic tests

The CO_2 hydrogenation kinetic experiments were performed in a high pressure fixed-bed vertically positioned tubular stainless steel reactor (VINCI Technologies, France) having an inner diameter of 1.27 cm and length of 21.5 cm. 1.0 g of the composite catalyst (2:1 mass ratio of In_2O_3 and commercial Silica mixture) was packed inside the reactor which was equipped with a thermocouple and held in place by thin layers of quartz wool both up- and downstream from the catalyst. The catalyst was positioned at the vertical center position of the reactor such that the thermocouple tip was in contact with the catalyst bed. The total depth of the composite catalyst bed was 1.4 cm. The remaining portions of the reactor were filled with SiC (500 μm size particles). The total volume of the reactor was 12.1 cm^3. The reactor was placed inside a furnace. H_2 and CO_2 were fed through separate mass flow controllers upstream from the reactor. Before reaction, the catalyst was pretreated by heating at a ramp rate of 5 ℃ min^{-1} and maintained at 400 ℃ for 1 h in Ar flow at 150 NmL min^{-1}. The reactor was then allowed to cool down to the desired reaction temperature in Ar flow before the feed gas was switched to CO_2 and H_2 and pressurized to the desired total pressure. Tests were conducted at a temperature of 200–400 ℃, a total pressure of 20–40 bar and with different H_2:CO_2 molar feed ratios from 2:1–6:1. By varying the total molar feed rate, the resulting variation in Weight

Hourly Space Velocity (WHSV) was from 6000 to 16000 mL g_{cat}^{-1} h^{-1}. The effluent gas from the reactor was quantitatively analyzed online using a gas chromatograph (GC, SCION 456) equipped with both thermal conductivity (TCD) and flame ionization detectors (FID). Immediately downstream from the reactor, a back pressure regulating valve reduced the pressure of the gas to near atmospheric pressure before it flowed into a condenser at room temperature. If the partial pressure of water exceeded its vapor pressure, water condensed and the effluent gas after the condenser was saturated with water. Based on mass balance calculations, it was found that water condensation occurred only at conditions with the conversion of CO_2 exceeding ca. 10%. Partial pressures of methanol in the effluent gas were always well below its vapor pressure. The possible condensation of water was accounted for, in order to rectify the simulated effluent gas composition with the experimental measurements. The GC was calibrated with varying concentrations of absolute methanol, CO_2, CO and CH_4. The calibration curves of CO_2 and methanol are presented in **Fig. S1** in Supplementary Information (SI). All calculations were performed with the data collected after the steady-state conditions were obtained. Carbon balances calculated were all greater than 95% for each experiment. The experimental error range was measured by repeating certain experimental reaction conditions.

CO_2 conversion (X_{CO_2}) was calculated based on the molar flow rates as:

$$X_{CO_2} = \frac{F_{CO_2,in} - F_{CO_2,out}}{F_{CO_2,in}} \times 100\% \quad (4)$$

where $F_{CO_2,in}$ and $F_{CO_2,out}$ are the molar CO_2 flow rates at the inlet and outlet respectively.

The selectivities to the main product methanol (S_{CH_3OH}) and side products CO (S_{CO}) and CH_4 (S_{CH_4}) are calculated as follows:

$$S_{CH_3OH} = \frac{F_{CH_3OH,out}}{F_{CO_2,in} - F_{CO_2,out}} \times 100\% \quad (5)$$

$$S_{CO} = \frac{F_{CO,out}}{F_{CO_2,in} - F_{CO_2,out}} \times 100\% \quad (6)$$

$$S_{CH_4} = \frac{F_{CH_4,out}}{F_{CO_2,in} - F_{CO_2,out}} \times 100\% \quad (7)$$

where $F_{CH3OH,out}$, $F_{CO,out}$, and $F_{CH4,out}$ are the corresponding outlet molar flow rates of methanol, CO and CH_4 respectively. The component molar flow rates were calculated from the measured gas compositions by mass balance calculations and accounting for the possible condensation of H_2O as explained above.

2.4. Modeling methods

2.4.1. Kinetic modeling

Single-site (competitive) and dual-site Langmuir–Hinshelwood kinetic models have been evaluated as alternatives. For the single-site model, it is assumed that the catalyst has only one type of active site (mainly the oxygen vacancies of In_2O_3) where both CO_2 and H_2 competitively adsorb [33]. H_2 is believed to adsorb dissociatively and the adsorption of methanol was assumed to be negligible. For comparison, a dual-site model has been considered to have two different sites for CO_2 and H_2 adsorption. The motivation behind considering a dual-site model is that the main active sites for CO_2 hydrogenation at a microscopic level are considered to be oxygen vacancies of In_2O_3, whereas, dissociative adsorption of H_2 can occur on In sites as shown in the DFT study by Ye et al. [31].

The model is based on three equilibrium reactions for (i) methanol synthesis (Eq. (1)), (ii) RWGS (Eq. (2)) and (iii) CO_2 methanation (Eq. (3)). Based on the reaction mechanism shown in Supplementary Information, the corresponding general kinetic rate expressions are given as:

$$r_{MeOH} = \frac{k_1 \frac{\left(P_{CO_2}.P_{H_2}^{\ 3} - \frac{P_{CH_3OH}.P_{H_2O}}{K_{eq,MeOH}}\right)}{P_{H_2}^{\ 2}}}{Inhibition\ term} \quad (8)$$

$$r_{RWGS} = \frac{k_2 \frac{\left(P_{CO_2}.P_{H_2} - \frac{P_{CO}.P_{H_2O}}{K_{eq,RWGS}}\right)}{\sqrt{P_{H_2}}}}{Inhibition\ term} \quad (9)$$

$$r_{CH_4} = k_3 \sqrt{P_{CO_2}} \sqrt{P_{H_2}} \frac{\left(1 - \frac{P_{CH_4}.P_{H_2O}^2}{P_{CO_2}.P_{H_2}^4.K_{eq,CH_4}}\right)}{Inhibition\ term} \quad (10)$$

where r_{MeOH}, r_{RWGS} and r_{CH_4} are the reaction rates for methanol synthesis, RWGS and methanation reactions respectively. k_1, k_2 and k_3 (in mol s^{-1} bar^{-1} kg_{cat}^{-1}) respectively represent the rate constants of the corresponding equations and $K_{eq,MeOH}$, $K_{eq,RWGS}$ and K_{eq,CH_4} (in bar^{-1}) are the equilibrium constants for each of the reactions. The values of the reaction equilibrium constants are calculated at the particular reaction temperatures from the Gibbs free energy of formation values reported in literature and correlations of heat capacities of the components. P_j corresponds to the partial pressure of each species j. The denominators of the rate equations are referred to as the inhibition terms. These reaction rates (Eq. 8–10) are applied for both the single- and dual-site models but using different inhibition terms, which are shown in Table 1. K_{CO_2} and K_{H_2} represent the adsorption equilibrium constants for CO_2 and H_2 respectively.

2.4.2. Reactor modeling technique

For the kinetic modeling, the reactor has been represented by a one-dimensional pseudo-homogeneous plug flow model considering the following assumptions: isothermal and isobaric conditions, steady-state regime, absence of axial dispersion and negligible mass transfer limitations. At low temperatures, the adiabatic temperature increase was a maximum of 13 °C, whereas, at the highest temperature, where the RWGS reaction was dominant, the adiabatic temperature decrease was up to 55 °C. However, during experiments, no deviations between the control temperature and the measured catalyst bed temperature were observed and hence heat transport was adequate to maintain isothermal reactor condition. The pressure drop in the reactor was calculated at typical conditions using the Ergun equation [34] and was in all conditions found to be less than a negligible value of ~ 0.04 Pa, allowing the reactor to be considered as isobaric. The mass transfer resistances of the reactants from the bulk gas to the catalyst particle surfaces and thereafter through the pores of the catalyst particles were evaluated by the Mears parameter (MP) and the Weisz-Prater parameter (WP) respectively. It was found that for all the reaction temperatures, MP was less than 0.0015 (MP < 0.0015) indicating that the external mass transfer could be neglected. In addition, the values of WP only approached 0.1 at the highest reaction temperature (WP < 0.1), and thus also internal diffusion resistance could be neglected. The variation of WP and MP with reaction temperatures (**Fig. S2**) and details regarding their calculations are given in the supplementary information.

The corresponding mass balance equation [8] is given by:

$$\frac{dF_j}{dw} = \sum_{i=1}^{n} v_{ij} r_i \quad (11)$$

Table 1
Inhibition terms for the single- and dual-site LHHW models.

Models	Inhibition term
Single-site	$\left(1 + K_{CO_2}.P_{CO_2} + \sqrt{K_{H_2}.P_{H_2}}\right)^2$
Dual-site	$\left(1 + K_{CO_2}.P_{CO_2}\right)\left(1 + \sqrt{K_{H_2}.P_{H_2}}\right)$

where w represents the catalyst weight, F_j the molar flow rate of species j, ν_{ij} the stoichiometric coefficient of species j in reaction i and r_i the rate of the reaction i.

2.4.3. Parameter optimization for the kinetic model

To minimize the high correlation between the pre-exponential factor and the activation energy, the reparametrized form of the Arrhenius equation has been used:

$$k_i = k_{i,ref}\exp\left(\frac{E_i}{R}\left(\frac{1}{T_{ref}}-\frac{1}{T}\right)\right) \quad (12)$$

where $k_{i,ref}$ is the reaction rate constant at the reference temperature T_{ref} and E_i is the activation energy. Also, to minimize the correlation between the adsorption equilibrium constants and the enthalpy of adsorption, the reparameterized form of the Van't Hoff equation was used:

$$K_i = K_{i,ref}\exp\left(\frac{\Delta H_i}{R}\left(\frac{1}{T_{ref}}-\frac{1}{T}\right)\right) \quad (13)$$

where $K_{i,ref}$ is the equilibrium constant at the reference temperature T_{ref} and ΔH_i is the enthalpy change. The reference temperature for all the calculations is 300 ℃, which is the average experimental temperature. The nonlinear least square function 'lsqnonlin' subroutine, based on the Levenberg-Marquardt method, in Matlab (MathWorks, Inc.) R2019b's optimization package was used for carrying out non-linear regression. This non-linear least square solver uses a gradient-based optimization method to minimize the residual sum of squares (SSR) function between the experimental and simulated results as shown in eq. 14 to optimize the kinetic parameters to find the best fit of model predictions to experimental measurements.

$$SSR = \sum_i \sum_j w_i \left(y_{i,j}^{exp} - y_{i,j}^{sim}\right)^2 \quad (14)$$

where $y_{i,j}^{exp}$ represents the experimental mole fractions of the species i in experiment j and $y_{i,j}^{sim}$ represents those calculated by numerical solution of the system of ordinary differential equations (Eq. (11)) that are solved by the ode15s solver using Matlab. w_i represents the weighting factor used typically to weigh up the residuals of species having lower concentrations. All components except H_2 and H_2O were included in the optimization.

Normalized sensitivity coefficients (S) for the parameters are calculated using eq. (15):

$$S = \beta_0 \frac{\sum\left(\frac{\Delta y^{sim}}{y_0^{sim}}\right)^2}{\Delta\beta} \quad (15)$$

where,

β_0 = parameter at its optimal value

$\Delta\beta$ = change in parameter from optimal value

y_0^{sim} = simulated mole fraction value at an optimal value of the parameter

Δy^{sim} = change in simulated mole fraction due to change in the parameter value

3. Results and discussion

3.1. Catalyst characterization

Fig. 1**a** shows the XRD pattern of the as-prepared In_2O_3 catalyst. Distinct peaks corresponding to body-centered cubic In_2O_3 confirm the crystalline nature of the sample. The diffraction peaks at 21.5°, 30.7°, 35.5°, 37.8°, 41.9°, 45.8°, 51.05°, 56.1°, 60.8°, 63.7°, 68.0° and76.3°

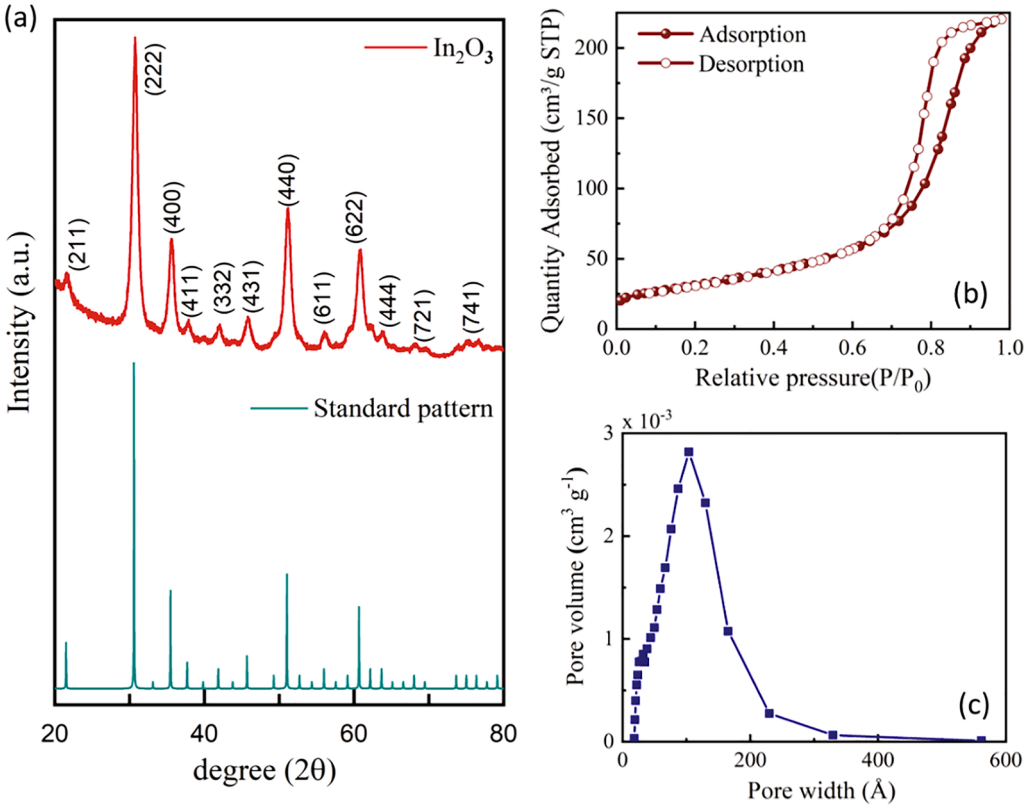

Fig. 1. (a) XRD pattern, (b) BET adsorption–desorption isotherm and (c) pore size distribution of In_2O_3 catalyst.

correspond to the (2 1 1), (2 2 2), (4 0 0), (4 1 1), (3 3 2), (4 3 1), (4 4 0), (6 1 1), (6 2 2), (4 4 4), (7 2 1) and (7 4 1) planes respectively (ICDD 01–088-2160) [3]. The corresponding standard pattern has also been shown. The average crystallite size of 10 nm was calculated using the Scherrer equation from the (2 2 2) diffraction peak.

The specific surface area of the In_2O_3 catalyst as measured from the nitrogen adsorption–desorption isotherm was 112 $m^2\ g^{-1}$ (Fig. 1**b**). An average pore size of 9.5 nm and a total pore volume of 0.34 $cm^3\ g^{-1}$ was obtained (Fig. 1**c**). The adsorption–desorption curve shows type IV isotherm characteristics having a prominent hysteresis loop in the relative pressure (P/P_0) range of 0.6–1, signifying its mesoporous structure.

To get a deeper insight into the morphology of the as-prepared In_2O_3 catalyst, a high resolution TEM analysis has been performed (Fig. 2**a-c**). The lattice fringes with an interplanar spacing of 0.291 nm corresponding to the (2 2 2) plane agree with the reported literature (Fig. 2**d**) [3]. A particle size distribution is shown in Fig. 2**e**, where the average diameter of the In_2O_3 particles (as estimated from the TEM image shown in Fig. 2b) is approximately 16.4 nm. However, some of the 10–20 nm particles shown in TEM have aggregated together to form larger particles which appear to be 30 nm or more. These large agglomerates were not included in the estimation of the average particle size. The SEM images of In_2O_3 are shown in **Fig. S3** in the Supplementary Information, which also shows large aggregated clusters with the aggregates varying in sizes up to at least 1 μm. The as-prepared and spent In_2O_3 catalysts were analyzed using TEM and XPS, to determine chemical and morphological differences before and after the reaction. These results are shown in **Figs. S4 and S5** in the Supplementary Information. The average particle size slightly increased from 16.4 nm (before reaction) to 17.7 nm (after reaction) as can be seen from the TEM particle size distribution graphs (**Figs. S4c and f**). XPS was performed on the argon pretreated In_2O_3 catalyst to study the possible change in reactivity due to oxygen vacancies before and after the CO_2 hydrogenation reaction. The catalyst pretreatment was done at 400 °C for 1 h in Ar atmosphere before CO_2 hydrogenation activity measurements because it has been reported in the literature that this thermal treatment can favorably lead to the formation of oxygen vacancies on the catalyst [35]. From the deconvoluted O1s XPS spectra shown in **Fig. S5,** it was found that the fresh catalyst has 22% oxygen vacancies which reduced to 16.5% after CO_2 hydrogenation in the spent catalyst. Our results are consistent with those reported by Martin et al. [28] where they have mentioned that a substantial drop in the surface area and noticeable sintering can be the probable reasons behind the reduction in the number of oxygen defects after CO_2 hydrogenation over the In_2O_3 catalyst [28,36].

3.2. Kinetic analysis

To study the kinetics of the reaction mechanism, a series of experiments have been carried out. All the kinetic experiments were carried out under steady-state conditions. A broad range of experimental conditions was examined to provide a good basis for data for the kinetic model. The reaction conditions and the corresponding CO_2 conversions and product selectivities for the catalytic hydrogenation of CO_2 are summarized in Table 2. Here the four main experimental conditions that have been varied are a) temperature (Exp. 1a–1e), b) pressure (Exp. 2a–2c), c) H_2:CO_2 molar feed ratio (Exp. 3a–3e) and d) WHSV (Exp. 4a–4d). Experiments 5a–5o investigated the simultaneous variation of temperature and molar feed ratio. The standard reaction conditions are defined as T = 300 °C, P = 40 bar, WHSV = 9000 mL $g_{cat}^{-1}h^{-1}$ and molar H_2:CO_2 = 3:1. These conditions were repeated periodically throughout the experimental study in each experiment set (i.e. experiments 1c, 2c, 3b, 4b and 5 h). There were only small variations in the measured methanol conversion and product selectivities for these repeated experiments, which indicates the stability of the catalyst. From the catalyst characterization results in Section 3.1 above, it was observed that exposure of the catalyst to reaction conditions caused a slight increase in average particle size and a small decrease in the number of oxygen vacancies. Apparently, these changes occurred in the catalyst either very early after exposure to the reaction conditions or they were not sufficient to cause any significant changes in the catalyst performance. The small

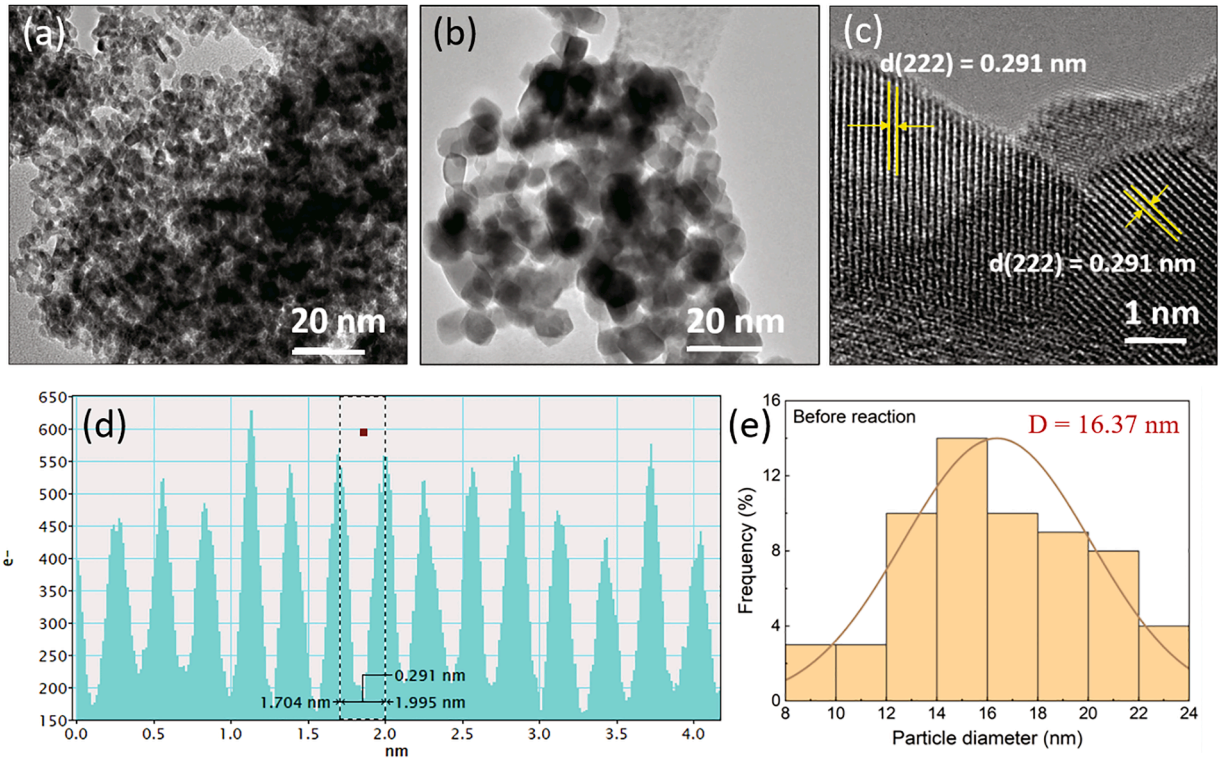

Fig. 2. HRTEM images (a-c), (d) the profile of the lattice fringes of In_2O_3 and (e) particle size distribution.

Table 2
Overview of reaction conditions and results of the catalytic hydrogenation of CO_2 over In_2O_3.

Exp	P (bar)	T (°C)	WHSV(mL g_{cat}^{-1} h^{-1})	H_2:CO_2	X_{CO2} (%)	S_{CH3OH}(%)	S_{CO}(%)	S_{CH4}(%)
1a	40	*200*	9000	3:1	0.15	100	0	0
1b	40	*250*	9000	3:1	1.56	79.70	20.30	0
1c	40	*300*	9000	3:1	6.27	66.31	33.09	0.60
1d	40	*350*	9000	3:1	11.79	30.01	68.66	1.33
1e	40	*400*	9000	3:1	22.52	1.25	97.26	1.49
2a	*20*	300	9000	3:1	4.25	57.23	42.00	0.76
2b	*30*	300	9000	3:1	5.11	62.54	36.74	0.72
2c	*40*	300	9000	3:1	5.92	66.24	33.12	0.64
3a	40	300	9000	*2:1*	3.59	65.61	33.81	0.58
3b	40	300	9000	*3:1*	5.65	66.02	33.36	0.62
3c	40	300	9000	*4:1*	7.23	66.76	32.56	0.68
3d	40	300	9000	*5:1*	8.79	67.40	31.86	0.74
3e	40	300	9000	*6:1*	10.34	67.99	31.20	0.81
4a	40	300	*6000*	3:1	6.75	66.25	33.05	0.70
4b	40	300	*9000*	3:1	5.74	64.99	34.35	0.66
4c	40	300	*12,000*	3:1	4.27	65.87	33.44	0.68
4d	40	300	*16,000*	3:1	3.37	65.15	34.18	0.67
5a	40	200	9000	2:1	0.08	100	0	0
5b	40	200	9000	3:1	0.13	100	0	0
5c	40	200	9000	4:1	0.15	100	0	0
5d	40	250	9000	2:1	0.96	73.13	26.87	0
5e	40	250	9000	3:1	1.35	78.29	21.71	0
5f	40	250	9000	4:1	1.77	80.40	19.60	0
5 g	40	300	9000	2:1	3.93	61.61	37.84	0.54
5 h	40	300	9000	3:1	5.84	66.34	32.95	0.71
5i	40	300	9000	4:1	6.79	69.79	29.63	0.57
5j	40	350	9000	2:1	11.51	27.18	71.06	1.76
5 k	40	350	9000	3:1	13.61	31.28	66.60	2.12
5 l	40	350	9000	4:1	16.59	35.15	62.59	2.26
5 *m*	40	400	9000	2:1	25.80	2.30	96.50	1.20
5*n*	40	400	9000	3:1	23.03	2.68	95.83	1.49
5o	40	400	9000	4:1	25.36	3.41	94.87	1.72

X_{CO2} = CO_2 Conversion; S_i = Selectivity for product i (calculated using eqs. (4) through (7))

deviations at the repeated standard reaction conditions were used to provide an estimate of the purely experimental variation of the results (Section 3.5 Figs. 5, 7, 8 and 9 show error bars for the experimental results). It was confirmed from the experimental findings that no dimethyl ether (DME) was formed under any conditions.

3.3. Analysis of experimental results

Although the methanation reaction (eq. (3)) is strongly thermodynamically favored, it can be seen from Table 2 that it is only a minor reaction at these conditions over In_2O_3, with a selectivity only reaching up to about 2.3%. Hydrogenation of CO_2 to methanol (eq. (1)) is an exothermic process, hence low temperature and high pressure thermodynamically favor the production of methanol. But at high temperatures, the RWGS reaction is both thermodynamically and kinetically favored as it is an endothermic reaction (eq. (2)). It has been observed that methanol synthesis from CO_2 hydrogenation over the In_2O_3 catalyst is usually accompanied by undesirable CO formation, specifically at higher temperatures [35]. Calculations for the simultaneous equilibrium for the methanol synthesis and RWGS reactions from CO_2 reveal that equilibrium CO selectivity reaches around 99.2% at 400 °C with the methanol selectivity dropping to around 0.77% (Fig. 3**a**). The experimental data also shows a similar trend for CO selectivity reaching as high as 97.3% with methanol selectivity dropping to 1.3% at 400 °C (Fig. 3**b**). However, due to kinetic limitations, the experimental CO_2 conversion is always lower than the thermodynamic values, even at higher temperatures, indicating that simultaneous equilibrium was never reached for these two reactions. Another significant observation is

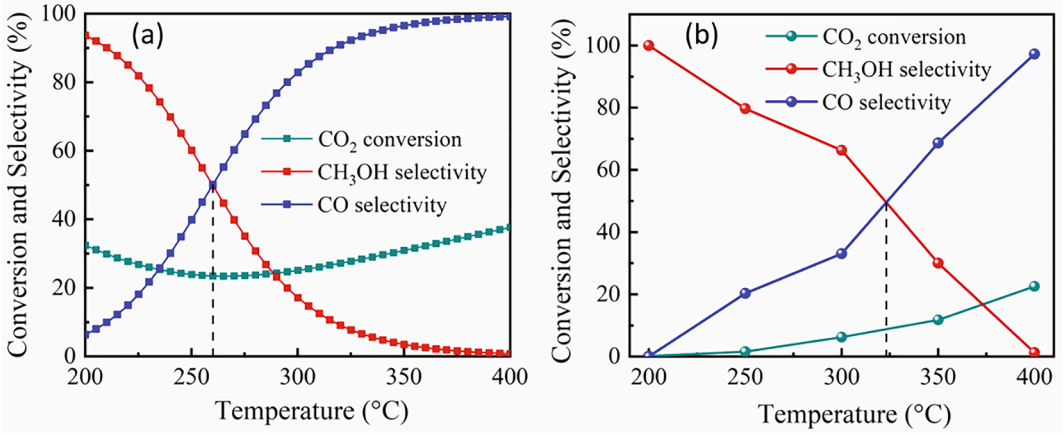

Fig. 3. (a) Calculated equilibrium conversion and selectivity for simultaneous methanol synthesis and RWGS reactions and (b) experimental data of CO_2 hydrogenation over In_2O_3 for varying temperatures at P = 40 bar, WHSV = 9000 mL $g_{cat}^{-1}h^{-1}$ and molar H_2:CO_2 = 3:1.

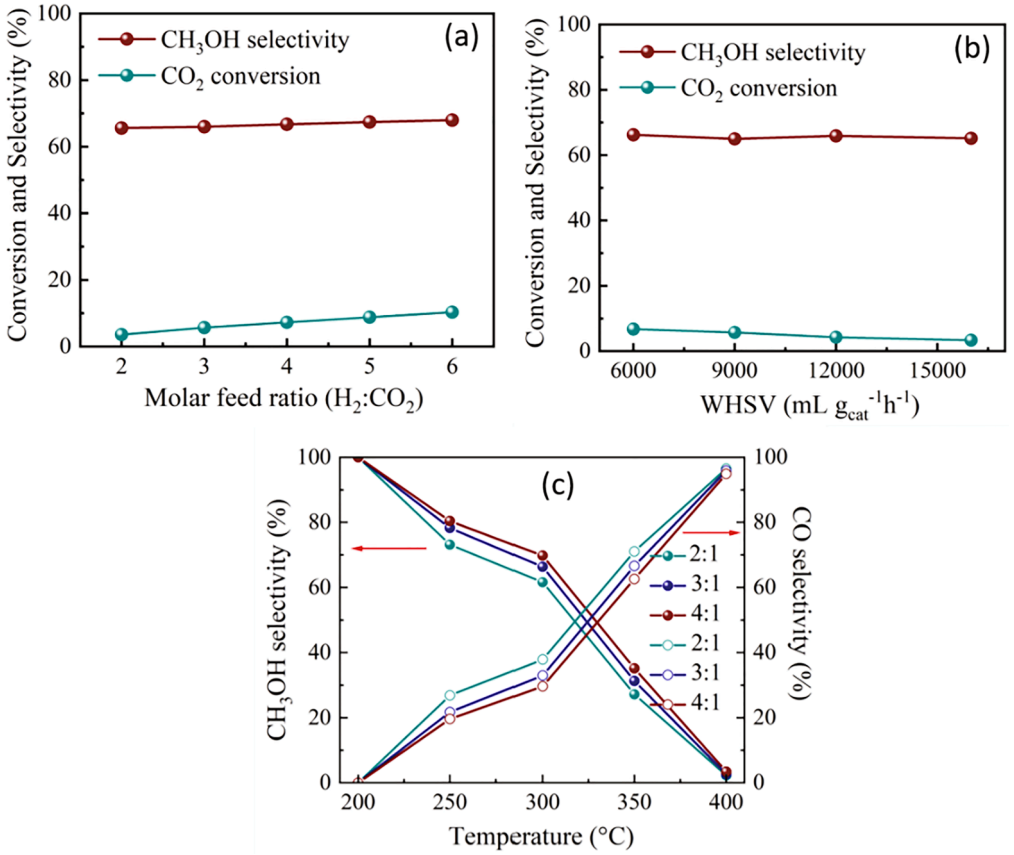

Fig. 4. Effect of (a) H_2:CO_2 molar feed ratio and (b) WHSV on CO_2 conversion and methanol selectivity over In_2O_3 and (c) simultaneous effect of temperature and H_2:CO_2 molar feed ratio on methanol and CO selectivity. Standard reaction conditions: 300 ℃, 40 bar, WHSV = 9000 mL g_{cat}^{-1} h^{-1} and molar H_2:CO_2 = 3:1.

that the 50% selectivity point for methanol and CO shifts to a higher temperature (320 ℃) for the experimental data points when compared to the thermodynamic calculation (260 ℃). So, as the reaction temperature increases from 200 ℃ to 400 ℃, methanol selectivity decreases significantly from 100% to 1.3% although CO_2 conversion increases simultaneously. We have observed a similar trend for our experimental data as that shown by Sun *et al.* with their spherical cubic-In_2O_3 nanoparticle catalyst [35].

. When the H_2:CO_2 ratio is increased from 2:1 to 6:1, the methanol selectivity reaches 68.0% at a CO_2 conversion of 10.3% (Fig. 4**a**). On the other hand, the higher the molar feed ratio, the higher is the CO_2 conversion but it is just the reverse in the case of increasing WHSV. As WHSV increases, CO_2 conversion reduces gradually. Methanol selectivity reaches 65.2% for WHSV of 16000 mL $g_{cat}^{-1}h^{-1}$ with a CO_2 conversion of 3.4% (Fig. 4**b**). Methanol selectivity enhances and CO selectivity diminishes with the increased molar H_2:CO_2 feed ratio at all reaction temperatures above 200 °C as shown in Fig. 4**c**. At any given temperature e.g. 300 ℃, the methanol selectivity increases from 61.6% to 69.8% and the CO selectivity drops from 37.8% to 29.6% when the molar flow ratio of H_2:CO_2 increases from 2:1 to 4:1. This implies that a higher concentration of hydrogen in the feed gas relative to CO_2 promotes methanol formation. But for very high as well as very low temperatures, this effect is less clear.

The catalytic hydrogenation of carbon monoxide is another possible route of methanol formation according to the reaction shown in eq. (16):

$$CO + 2H_2 \rightarrow CH_3OH \quad (16)$$

However, for our reaction conditions, we expect that it should be negligible because the amount of CO_2 is always much more than CO. At the reactor outlet, for reaction temperatures less than 350 ℃, the concentration of CO_2 is about 150 times more than CO and it decreases to about 3.5 times the amount of CO at the highest temperature of 400 ℃ when the RWGS becomes the dominating reaction. Therefore, we can consider that the dominating portion of methanol formed at these reaction conditions originates directly from CO_2 hydrogenation. In this work, we have not investigated the direct effect of water on the In_2O_3 catalyst since the presence of water in the feed is unlikely under practical conditions as mentioned by Frei et al. [3].

3.4. Determination of kinetic parameters

The optimization procedure described in Section 2.4.3 was used to determine the values of the kinetic parameters in the rate equations (8) to (10) using the single- and dual-site kinetic models. Only the optimized parameters resulting from the single-site model will be shown and discussed in depth in this section because it was found to be superior for describing the experimental data. A comparison of the performance of the kinetic models will be shown and discussed later in section 3.6. From a series of simulations, 10 parameters were estimated for each kinetic model: 3 rate constants (k_{ref}), 3 activation energies (E_a), 2 equilibrium adsorption constants (K_{ref}) and 2 heat of adsorptions (ΔH_a) pertaining to the methanol synthesis, RWGS and methanation reactions. The rate constants and equilibrium adsorption constants are determined at the reference temperature T_{ref} (300 ℃). The optimized parameter values are listed in Tables 3 and 4 for the single-site model. The corresponding parameters for the dual-site model are listed in **Tables S1 and S2** in Supplementary Information.

As shown in Table 2, the series 1 experiments (varying temperature) were important to obtain the rate constants and activation energies. The series 2 and 3 experiments (varying pressure and molar feed ratio) were important for determining the adsorption equilibrium constants and in turn their values established the effective order of the reactions. Then

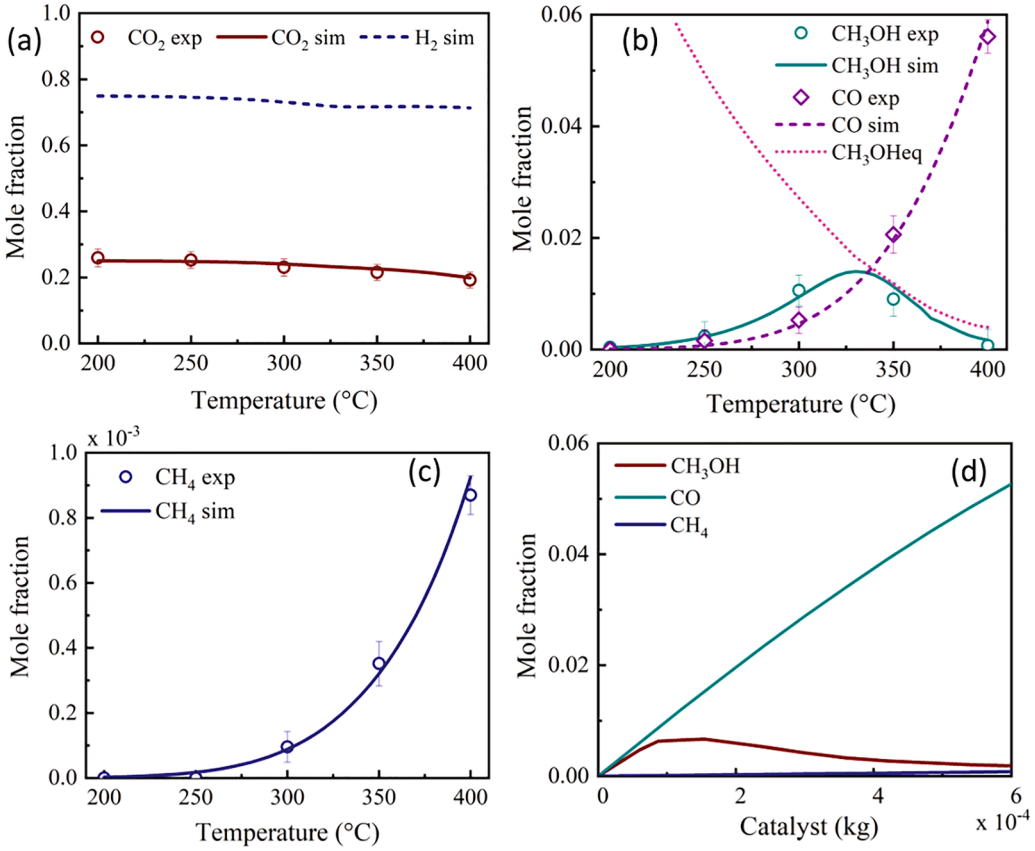

Fig. 5. Effect of temperature on the outlet mole fractions of (a) CO_2 and H_2, (b) CH_3OH and CO and (c) CH_4. and (d) mole fraction of CH_3OH, CO CH_4 as a function of catalyst weight at 400 °C. Standard reaction conditions: 40 bar, WHSV = 9000 mL g_{cat}^{-1} h^{-1} and molar H_2:CO_2 = 3:1. The experimental results are shown with symbols and the modeling results with lines.

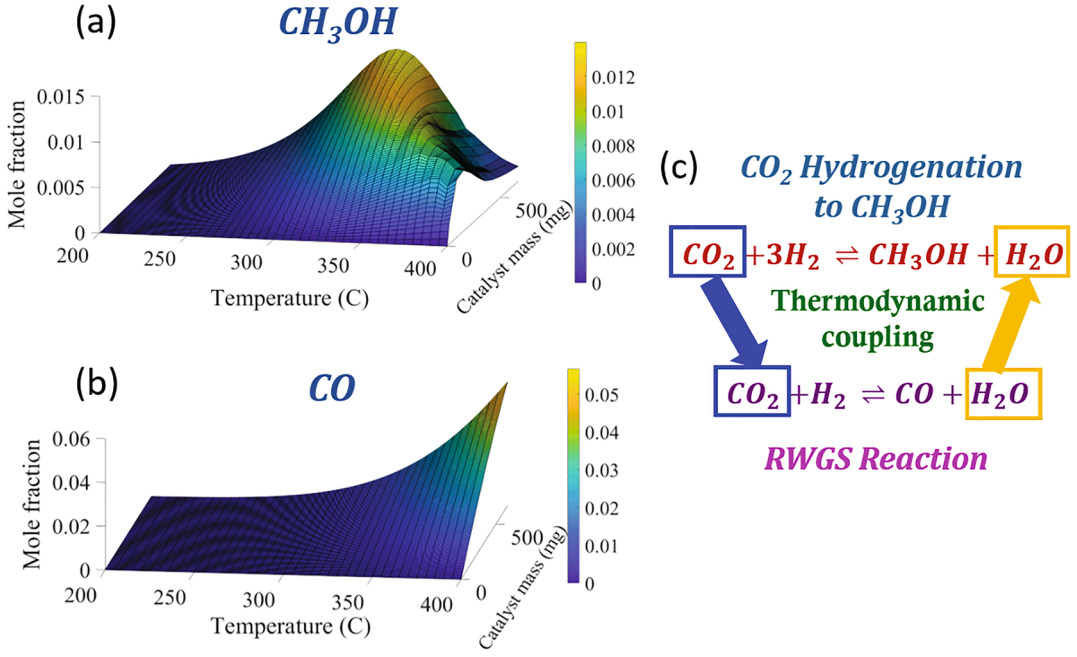

Fig. 6. Surface plots showing the change in mole fractions of (a) CH_3OH and (b) CO along the catalyst bed at varying temperatures and (c) thermodynamic coupling between the CO_2 hydrogenation to methanol and the RWGS reactions.

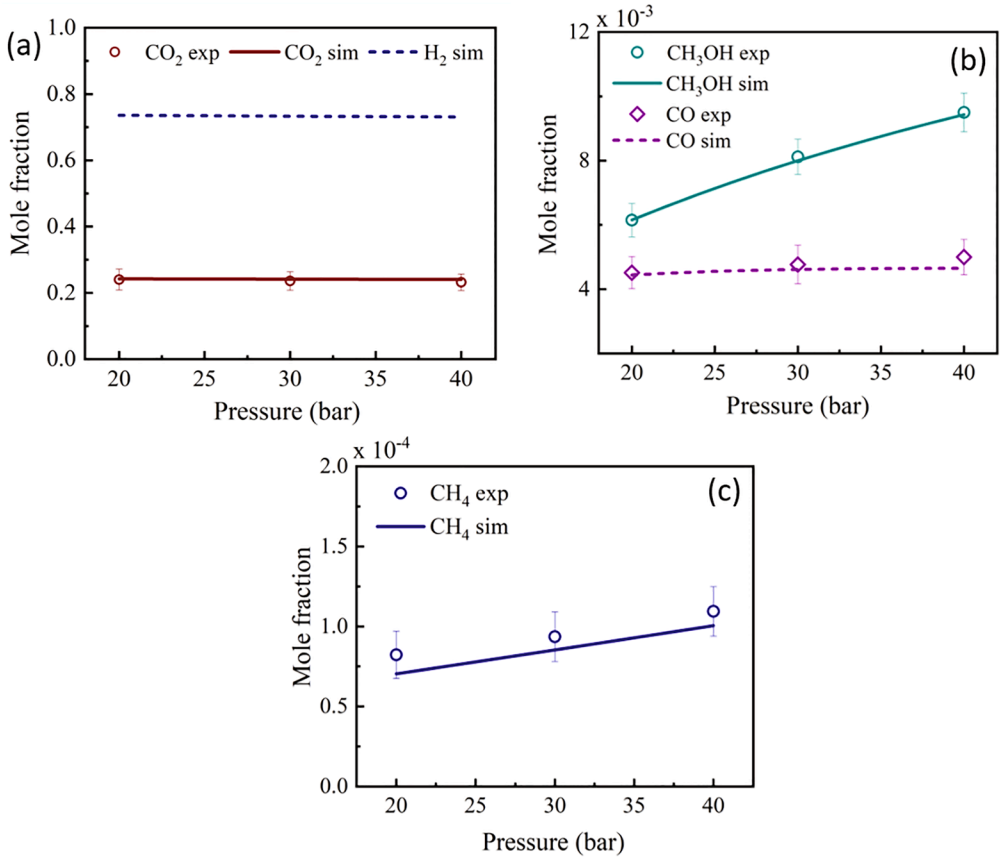

Fig. 7. Effect of total reactor pressure on the outlet mole fractions of (a) CO_2 and H_2, (b) CH_3OH and CO and (c) CH_4. Standard reaction conditions: 300 °C, WHSV = 9000 mL g_{cat}^{-1} h^{-1} and molar H_2:CO_2 = 3:1. The experimental results are shown with symbols and the modeling results with lines.

the series 5 experiments (both varying molar feed ratio and temperature) were important for determining the heats of adsorption (ΔH_a). There was also a correlation between parameters like for example between the rate constants and the adsorption equilibrium constants.

The parameter sensitivities in Tables 3 and 4, measure the influence that a parameter has on the model predictions. The sensitivities are obtained from a 0.1% change in each parameter and they are normalized with respect to the value of the parameter so that the sensitivities for each parameter can be compared (eq. (15)). A high sensitivity indicates that the experiments were appropriate to successfully resolve the value of a parameter. Whereas, a low sensitivity indicates the parameter value is more uncertain and it may even be excluded from the model. As we can see from Table 4, the sensitivity of the heat of adsorption value for H_2 was very low and as well the adsorption equilibrium constant for H_2 was less sensitive than that for CO_2. This indicates that the inhibiting effects of CO_2 were of greater importance for the predictions of the model than that of H_2 and the inhibiting effects for H_2 varied negligibly over the temperature range investigated when the molar feed ratios were simultaneously varied. It can also be noted that among the activation energies in Table 3, the activation energy for methanol synthesis had the lowest sensitivity. This is because, as will be shown below in section 3.5.1, the methanol synthesis reaction became equilibrium limited at higher reaction temperatures.

CO_2 hydrogenation over a defective In_2O_3 (1 1 0) surface with oxygen vacancies for methanol synthesis was investigated using DFT calculations as mentioned before. The adsorption energy of CO_2 was reported to be −0.61 eV (−56.8 kJ mol^{-1}) and that of H_2 to be −0.44 eV (−42.4 kJ mol^{-1}) [31]. The heat of adsorption (ΔH_a) values observed from our single-site model are −12.5 and −25.9 kJ mol^{-1} for CO_2 and H_2 respectively. These values are considerably lower than those reported by Ge *et al.* [31]. The probable reason behind this is that for the kinetic model reported here, the parameters for CO_2 and H_2 adsorption on the surface, must in fact account for the influence of many other adsorbed species like H_2O, CO, formate and other intermediate species formed from the reactants. Moreover, Frei *et al.* have derived apparent activation energies of 1.73 eV (166 kJ mol^{-1}) and 1.96 eV (189 kJ mol^{-1}) for CO_2 hydrogenation to methanol and the RWGS reaction respectively over In_2O_3 based on DFT simulations [3]. Our values of activation energies from the single-site model are lower (35.7 and 54.5 kJ mol^{-1} respectively) for these two reactions. In the formulation of an LHHW overall rate equation, the rate constants, shown here in eqs. (8) to (10), are lumped parameters that are a product of the rate constant of the rate-determining step and the adsorption equilibrium constants. As a result, these activation energies do not reflect the apparent activation energies of the reaction. Later in section 3.7, from an analysis of the experimental data, it can be shown that the apparent activation energies are greater (90 and 110 kJ mol^{-1}) than those in the single-site rate expressions but still lower than those reported by Frei *et al.* There could be different reasons for the differences, such as the DFT simulations were performed on (1 1 1) plane of In_2O_3, while our catalyst exhibited many different crystal planes and where (2 2 2) was dominating (as shown in Fig. 1**a**).

3.5. Comparison of experiments and kinetic model predictions

The developed single-site model was based on the effects of different reaction conditions (as shown in Table 2) in terms of temperature, pressure, molar feed ratio and WHSV on the catalytic performance of In_2O_3. All the plots in the following sections (Figs. 5 and 7-10) contain both the experimental data points (represented by symbols) as well as the simulation data (represented by lines) obtained from the model predictions.

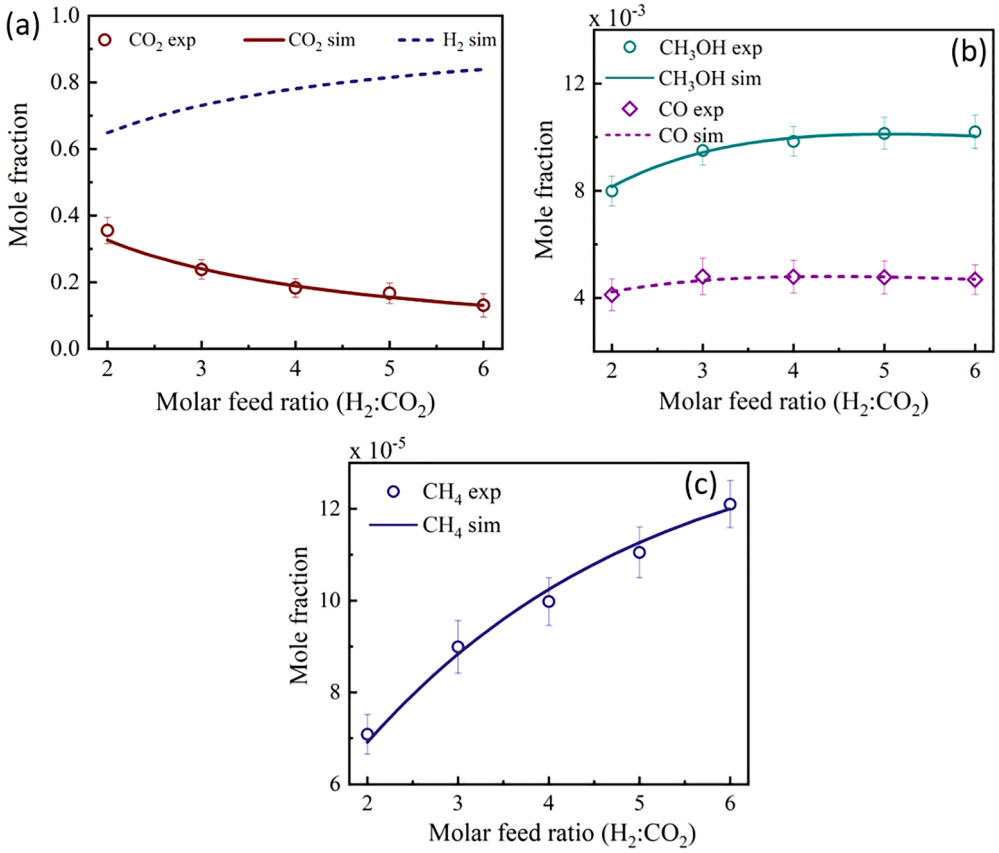

Fig. 8. Effect of molar feed ratio of H_2:CO_2 on the outlet mole fractions of (a) CO_2 and H_2, (b) CH_3OH and CO and (c) CH_4. Standard reaction conditions: 300 ℃, 40 bar and WHSV = 9000 mL g_{cat}^{-1} h^{-1}. The experimental results are shown with symbols and the modeling results with lines.

3.5.1. Effect of temperature

The reaction temperature has been varied between 200 and 400 ℃ mainly to investigate how the methanol synthesis and the competitive RWGS reactions (eqs. (1) and (2)) occur on the In_2O_3 surface over this range of temperature. Low temperature and high pressure favor methanol synthesis as the RWGS reaction is suppressed under these reaction conditions. At higher temperatures, the methanol selectivity largely reduces as the RWGS starts becoming more prominent. Fig. 5 shows the variation in outlet mole fractions of CO_2, H_2, CH_3OH, CO and CH_4 w.r.t. the reaction temperature. Both the outlet reactant concentrations (H_2 and CO_2) were found to reduce with the increase in temperature (Fig. 5**a**). The temperature has a considerable effect on the equilibrium conversion of CO_2 to methanol over the In_2O_3 catalyst. Our model shows that as temperature increases from 200 ℃, methanol concentration initially increases up to around 330 ℃, after which the methanol synthesis reaction reaches equilibrium and therefore the methanol concentration begins to drop (Fig. 5**b**). The equilibrium outlet methanol concentration from 235 to 400 ℃ is also shown for comparison (dotted line in Fig. 5**b**). It represents how much more methanol could have been produced, before thermodynamic equilibrium for methanol synthesis is reached, given the amount of CO already present from the RWGS reaction. It can be seen that below 330 ℃, the methanol synthesis is kinetically limited whereas above 330 ℃ it reaches thermodynamic equilibrium. The same equilibrium calculation was done for the RWGS reaction, i.e. how much more CO could have been produced was calculated given the amount of methanol already present. This result is not shown in Fig. 5b, but these amounts were in all cases well above the experimental outlet CO mole fractions. On the other hand, temperature favors the RWGS reaction as it is an endothermic reaction and therefore our model shows that with the increase in temperature, at least up to 400 ℃, the concentration of CO in the outlet increases and remains within the kinetic regime rather than reaching thermodynamic equilibrium (Fig. 5**b**). The error bars around the experimental data points in Fig. 5 indicate the estimated variation in the experimental measurements from repeated experiments. A strength of this single-site kinetic model is that the deviations of the model predictions are largely always within the range of the estimated experimental variation. The model also shows that the methanation reaction is also favored with the increase in temperature (Fig. 5**c**). According to the model, initially, the rate of methanol synthesis is almost equal to that of RWGS at 400 °C (Fig. 5**d**). But then eventually after a small amount of catalyst mass (1×10^{-4} kg), the methanol synthesis reaches equilibrium in the simulations, but the RWGS reaction continues. So, at 400 ℃ it could be possible to achieve a higher selectivity for methanol, with a higher WHSV.

The surface plots, shown in Fig. 6**,** give a clearer picture of the variation of methanol and CO concentrations along the catalyst bed at varying temperatures as discussed in Fig. 5b. Our single-site model shows that methanol concentration increases with catalyst mass up to about 330 ℃ after which it reaches a maximum, then it remains constant till 350 ℃ as it reaches thermodynamic equilibrium, and finally, above 350 ℃ its concentration decreases with high catalyst mass. This is because simultaneously the concentration of CO is increasing and the RWGS reaction causes CO_2 to decrease and H_2O to increase. This H_2O produced from the RWGS reaction can further react with the methanol formed already from the CO_2 hydrogenation reaction and can shift the equilibrium for CH_3OH synthesis backward. So, at high temperature, the progress of the RWGS reaction causes the methanol synthesis reaction to reverse, so that methanol steam reforming begins to occur as CO concentration increases (Fig. 6**a**). The CO_2 formed from methanol steam reforming can either help in the forward reaction of methanol synthesis again or can also assist RWGS reaction. On the other hand, the CO concentration at all temperatures simply always increases with the

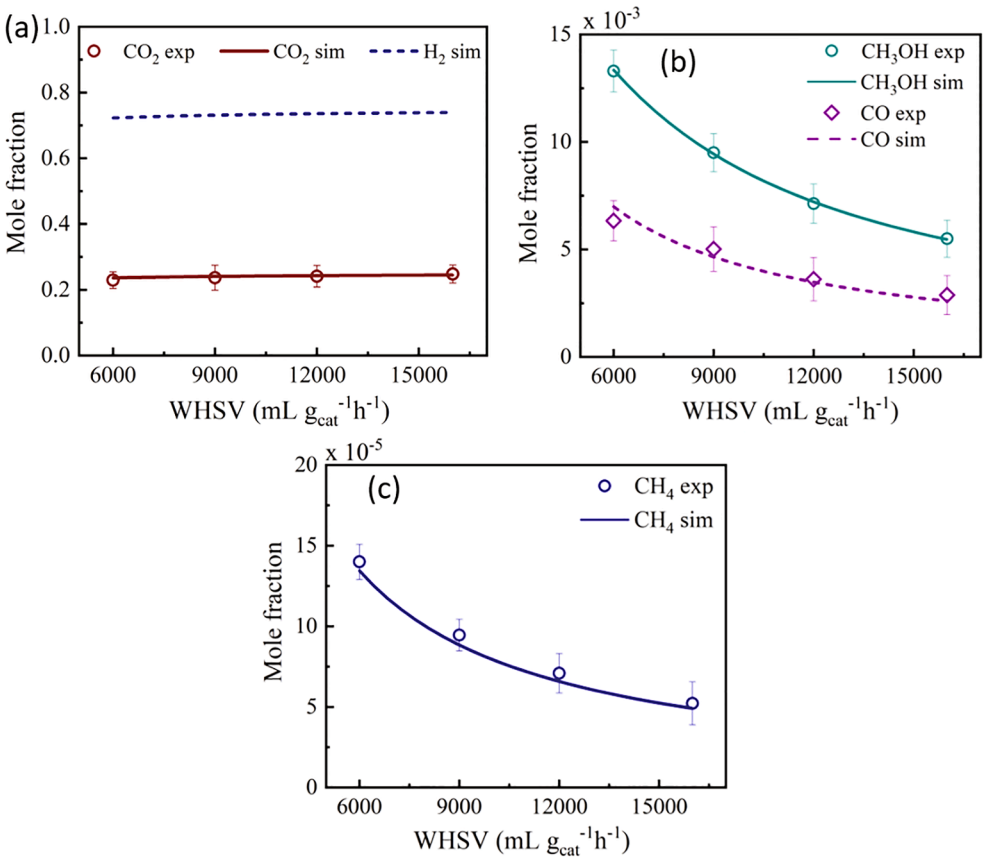

Fig. 9. Effect of WHSV on the outlet mole fractions of (a) CO_2 and H_2, (b) MeOH and CO and (c) CH_4. Standard reaction conditions: 300 ℃, 40 bar and molar H_2:CO_2 = 3:1. The experimental results are shown with symbols and the modeling results with lines.

Table 3
Optimized rate constants and activation energies along with their sensitivity coefficients obtained from the single-site kinetic model for the In_2O_3 catalyst.

Reactions	*k_{ref} (mol s^{-1} bar^{-n} kg_{cat}^{-1}) at 300 °C	Normalized sensitivity	E_a(kJ mol^{-1})	Normalized sensitivity
CH_3OH	6.9×10^{-4}	0.022	35.7	0.012
RWGS	1.8×10^{-3}	0.038	54.5	0.059
Methanation	1.1×10^{-4}	0.032	42.5	0.026

* Regarding units for k_{ref} for CH_3OH synthesis n = 2; RWGS n = 1.5; Methanation n = 1.

Table 4
Adsorption constants and enthalpy of adsorption along with their sensitivity coefficients obtained from the single-site model for the In_2O_3 catalyst.

Parameters	H_2	Normalized sensitivity	CO_2	Normalized sensitivity
K_{ref}(bar^{-1}) at 300 °C	0.76	0.013	0.79	0.129
ΔH_a (kJ mol^{-1})	−12.5	8.0×10^{-4}	−25.9	0.053

catalyst mass (Fig. 6**b**). This result corroborates with observations that In_2O_3 is highly active and selective toward CO_2 in methanol steam reforming [37]. Fig. 6**c** illustrates how the RWGS and methanol synthesis reactions are thermodynamically and also kinetically coupled through CO_2 and H_2O concentrations.

3.5.2. *Effect of pressure*

Reaction pressure also plays a significant role in methanol synthesis from CO_2 hydrogenation over the In_2O_3 catalyst. The pressure effect was investigated in the 20–40 bar range with the reactor operating at a constant temperature of 300 ℃, WHSV of 9000 mL g_{cat}^{-1} h^{-1} and molar feed ratio of H_2:CO_2 = 3:1 (as shown in Fig. 7). An increase in total pressure thermodynamically favors CO_2 conversion to methanol, whereas, the equilibrium for the RWGS reaction is unaffected by pressure. As can be seen from Fig. 5**b**, at 300 ℃ and the highest pressure (40 bar), both reactions are still operating within the kinetic regime. We have calculated that at 40 bar, the outlet methanol reaches 13% of the equilibrium, whereas at 20 bar it reaches 34% of equilibrium for methanol synthesis. Thus, the experiments in Fig. 7 are all within the kinetic regime for methanol synthesis. As a result, the improved selectivity for methanol at higher pressure, as evident from Fig. 7**b**, is not purely a result of thermodynamic effects, and instead, some kinetic effect must be present. Apparently, an increase in the total pressure results in higher adsorption of CO_2 and H_2 on the In_2O_3 surface and this favors higher methanol production. The simulated data points from the model fitted well with the experimental data. The model shows that CO production is less affected by the enhancement in pressure, but CH_4 concentration substantially increases with an increase in total pressure (Fig. 7**c**), although still at low levels.

3.5.3. *Effect of molar feed ratio*

Since both H_2 and CO_2 at different stoichiometric ratios are the main reactants for both the CO_2 hydrogenation to methanol and the RWGS reactions, the variation in the H_2/CO_2 molar feed ratio can significantly affect the kinetics of both reactions. The H_2:CO_2 molar feed ratio was varied from 2:1 to 6:1 with a constant reactor temperature of 300 ℃, at a pressure of 40 bar and WHSV 9000 mL g_{cat}^{-1} h^{-1} as shown in Fig. 8. The model and experiments show that increasing the H_2 partial pressure while decreasing CO_2 partial pressure, favors CO_2 hydrogenation to

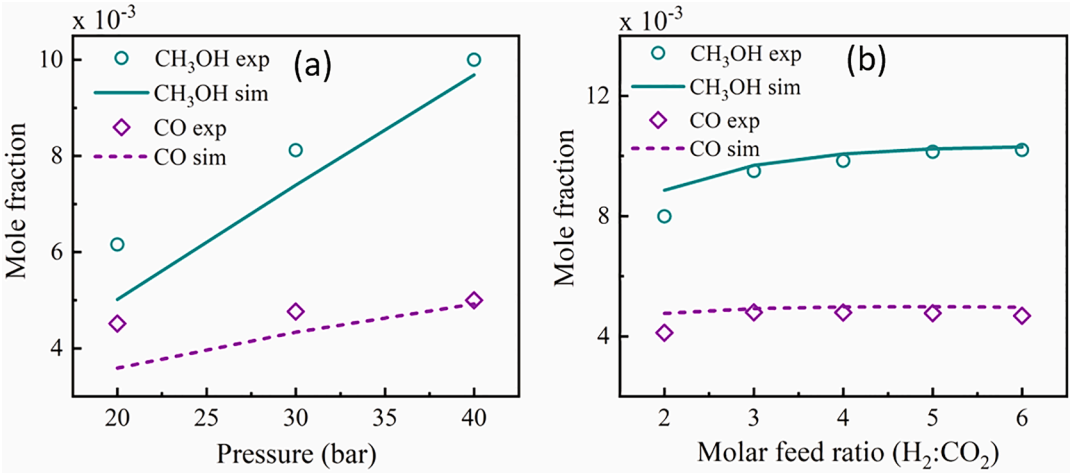

Fig. 10. Comparison of simulated and experimental data using the dual-site Langmuir Hinshelwood model to predict the effects of (a) pressure and (b) molar feed ratio on the outlet mole fraction of CH_3OH and CO. The experimental results are shown with symbols and the modeling results with lines.

methanol over the formation of CO as the H_2/CO_2 ratio is increased up to 4:1 (Fig. 8**b**). Further enhancement of the H_2/CO_2 ratio has less of an effect on the formation of methanol and the outlet mole fractions of CH_3OH as well as CO become more or less constant thereafter. An increase in the concentration of hydrogen in the feed with a proportionate decrease in CO_2 in the feed also favors the methanation reaction (Fig. 8**c**), but it should be noted that the methane formation is very low. The model also predicted well the effect of simultaneous variation of temperature and molar feed ratio on the moles of products formed which showed the robustness of our kinetic model (**Fig. S6**). These experiments (**Fig. S6**) were most important for determining ΔH_a (or the temperature dependence) of the adsorption equilibrium constants.

3.5.4. *Effect of WHSV*

A higher WHSV corresponds to a lower residence time of the reactants inside the reactor. The experimental results that are shown here agree with observations in literature that selectivity for methanol can be tuned by adjusting the WHSV [28]. The WHSV has been varied from 6000 to 16000 mL g_{cat}^{-1} h^{-1} by varying the flow rates of the reactants (Fig. 9). An increase in WHSV results in a decrease in the outlet mole fraction of both CH_3OH and CO, with a slight reduction in the selectivity for methanol. Our model predicts well the experimental data obtained by the variation of WHSV. It also reproduces the observed reduction in the yield of methane.

3.6. *Comparison with a dual-site model*

A dual-site Langmuir Hinshelwood model was also examined. However, the dual-site model was less effective than the single-site model for reproducing, in particular, the experimental data involving variations in total pressure and the molar feed ratios. The model predictions for these experiments are most sensitive to the adsorption equilibrium constants and the resulting effective order of the reactions with respect to CO_2 and H_2. In the single-site model, both CO_2 and H_2 molecules competitively adsorb at a single site on the catalyst surface. As mentioned before, DFT studies show that the oxygen vacancy sites on defective In_2O_3(1 1 0) surface assists CO_2 activation and hydrogenation to form methanol, whereas H_2 helps to generate the vacancies [31]. This was our motivation to compare the single-site and dual-site models. Fig. 10 shows the optimized predictions of the dual-site model. As can be seen from Fig. 10 w.r.t. the total pressure and molar feed ratio, the dual-site model predictions did not correlate as well with the experiments compared to the single-site model as shown in Fig. 7**b and** Fig. 8**b**.

The Pearson correlation coefficient (R-Pearson) and the weighted SSR values as shown in Table 5 indicate that the predictions of the single-site model are only very slightly better correlated to experimental results than those of the dual-site model. Except for the results shown in Fig. 10, the quality of fit of the models to other results was comparable.

Table 5
Comparison of statistics for the single- and dual-site models.

Model	R-Pearson	Weighted SSR
Single-site model	0.8684	7.84×10^{-3}
Dual-site model	0.8665	7.52×10^{-3}

3.7. *Kinetic analysis*

The apparent reaction orders were calculated from the reaction rates predicted by the optimized single-site kinetic model at varying conditions of partial pressures of the reactants (Fig. 11**a and b**). The absolute partial pressures of H_2 and CO_2 were varied about mean values ($P_{H2,mean}$ and $P_{CO2,mean}$) of 30.8 and 10.3 bars respectively, which are comparable to their feed partial pressures at 40 bar (gauge) experiments with a 3:1 molar feed ratio. The methanol and RWGS reaction orders were found to be 0.6 and 0.1 respectively w.r.t. hydrogen, whereas, w.r.t. CO_2 the orders of these reactions were nearly zero. Significantly w.r.t. the CO_2 partial pressure, the reaction rates initially increase and then slightly decrease indicating a varying order. This varying dependence is possible for a Langmuir Hinshelwood model, but not a power-law model. In particular with the single-site model, as opposed to the dual-site model, the reaction rates can first increase and later decrease with increasing P_{CO2}, with a sufficiently high value for the adsorption equilibrium constant for CO_2 (K_{CO2}). This suggests that initially at low P_{CO2}, there is an abundance of free sites on the surface of In_2O_3 and as P_{CO2} increases, the coverage of CO_2 on the surface increases without affecting the coverage of H_2, which leads to higher reaction rates. However gradually with increasing P_{CO2}, the availability of free sites becomes scarce and then at even higher P_{CO2}, the surface coverage of H_2 may be forced to decrease as CO_2 becomes the dominant adsorbent. The better fit of the single-site kinetic model and the apparent reaction orders observed here suggest that high CO_2 partial pressures can have an inhibiting effect on the reaction rates. Fig. 11**c** shows how the reaction rates for the single-site kinetic model vary with the molar feed ratio of H_2:CO_2. The reaction rates are nearly constant for molar H_2:CO_2 ratios greater than 4:1, but then more sharply decrease for lower ratios. It is demonstrated that the methanol and CO concentrations in Fig. 8**b** vary exactly in a similar way as the rate of the reaction w.r.t. the molar feed ratio as shown in Fig. 11**c**. These results suggest that the resulting effective reaction orders, possible

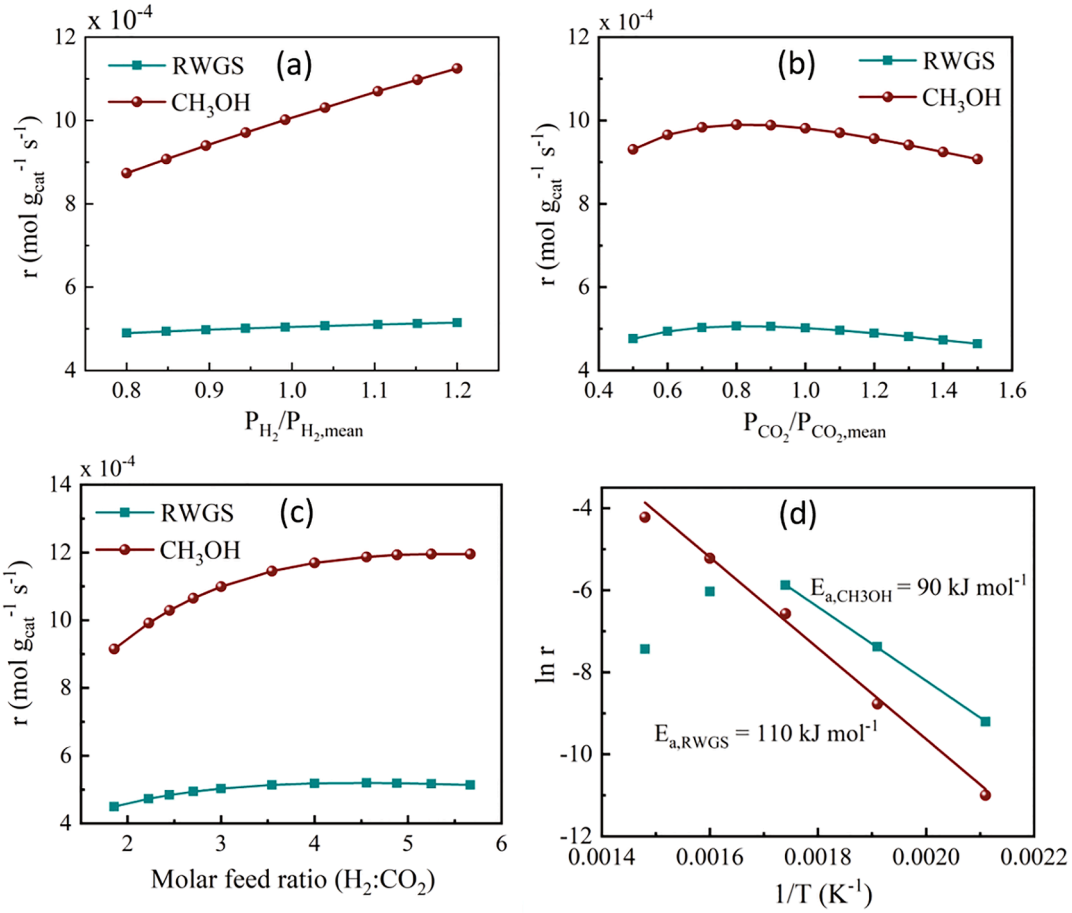

Fig. 11. Determination of the apparent reaction orders w.r.t. (a) partial pressure of H_2 and (b) partial pressure of CO_2 (c) Effect of H_2/CO_2 molar feed ratio on rates from single-site kinetic model and (d) Arrhenius plot for CO_2 hydrogenation to methanol and RWGS over In_2O_3 catalyst derived from experiment reaction rates.

with the single-site model, were important for reproducing the variation in selectivity with the molar feed ratio. The superiority of the single-site model could be because, for the single-site model, the reaction rates for methanol synthesis and the RWGS reaction first increase and then decrease at different ranges of the partial pressure of CO_2 (Fig. 11**b**), resulting in a variable order w.r.t. CO_2 that is not possible with the dual-site model. However, the single-site model does not disprove the theory that CO_2 reacts on the oxygen vacancies as predicted by DFT simulation studies. It might be possible that CO_2 and H_2 can compete for adsorption on most of the sites and then CO_2 preferentially reacts further on the oxygen vacancy sites to form methanol. To estimate the apparent activation energies for CO_2 hydrogenation to methanol and RWGS reactions, the Arrhenius plot is presented based on the experimental reaction rates. Apparent activation energies of 90 kJ mol^{-1} and 110 kJ mol^{-1} were derived for the methanol synthesis and RWGS reactions respectively (Fig. 11**d**). Some of the points in Fig. 11d for the methanol synthesis at the highest temperatures are not linear. This is because the methanol synthesis became equilibrium limited at high temperatures. As a result, the activation energy for methanol synthesis is only calculated from the 200–300 ℃ temperature range. The lower activation energy for methanol synthesis indicates that the In_2O_3 catalyst mediates methanol synthesis over the RWGS reaction [38]. The reaction rates, in this case, have been directly calculated from the experimental data. These results are very close to those obtained by Frei *et al.* from their experiments with the In_2O_3 catalyst. They have reported, apparent activation energies of 103 kJ mol^{-1} and 117 kJ mol^{-1} for methanol synthesis and RWGS reactions respectively [3]. The activation energies obtained from the kinetic model are much lower (35.7 and 54.5 kJ mol^{-1} respectively), although the activation energy for methanol synthesis is lower than the RWGS reaction. This is because in the LHHW kinetic model there are inhibition terms that decrease with temperature due to ΔH_a values, which also effectively increase the reaction rates with temperature.

Fig. 12 shows a series of parity plots for the outlet mole fractions of CO_2, CH_3OH, CO and CH_4 comparing the experimental data with the corresponding simulated results. The experimental data set consists of all the experimental data from 1a to 4d as shown in Table 2, used for optimizing the kinetic model. The experimental data points corresponding to (□) are the additional validation experiments listed in Table S3 in the Supplementary Information at other varying conditions that are not used for model optimization. The parity plots showed good agreement between the experimental mole fractions of each of these species and those calculated by the model, thereby showing that the single-site kinetic model predicts the data with good accuracy.

4. Conclusions

This work includes a kinetic study of CO_2 hydrogenation to methanol over an In_2O_3 catalyst taking into consideration two significant competitive reactions, namely the RWGS and methanation reactions. The catalytic reactions have been performed in an isothermal fixed-bed stainless steel tube reactor with a temperature ranging between 200 and 400 ℃, a total pressure between 20 and 40 bar and for varying H_2:CO_2 molar ratios (2:1–6:1) and different WHSV (6000–16000 mL g_{cat}^{-1} h^{-1}). A single-site kinetic model based on the LHHW rate equations is presented assuming that both CO_2 and H_2 can competitively adsorb on the same site that can predict the trends in the experimental data very well. The model predicts that at high temperature the progress of the RWGS reaction causes the methanol synthesis reaction to reverse, so that

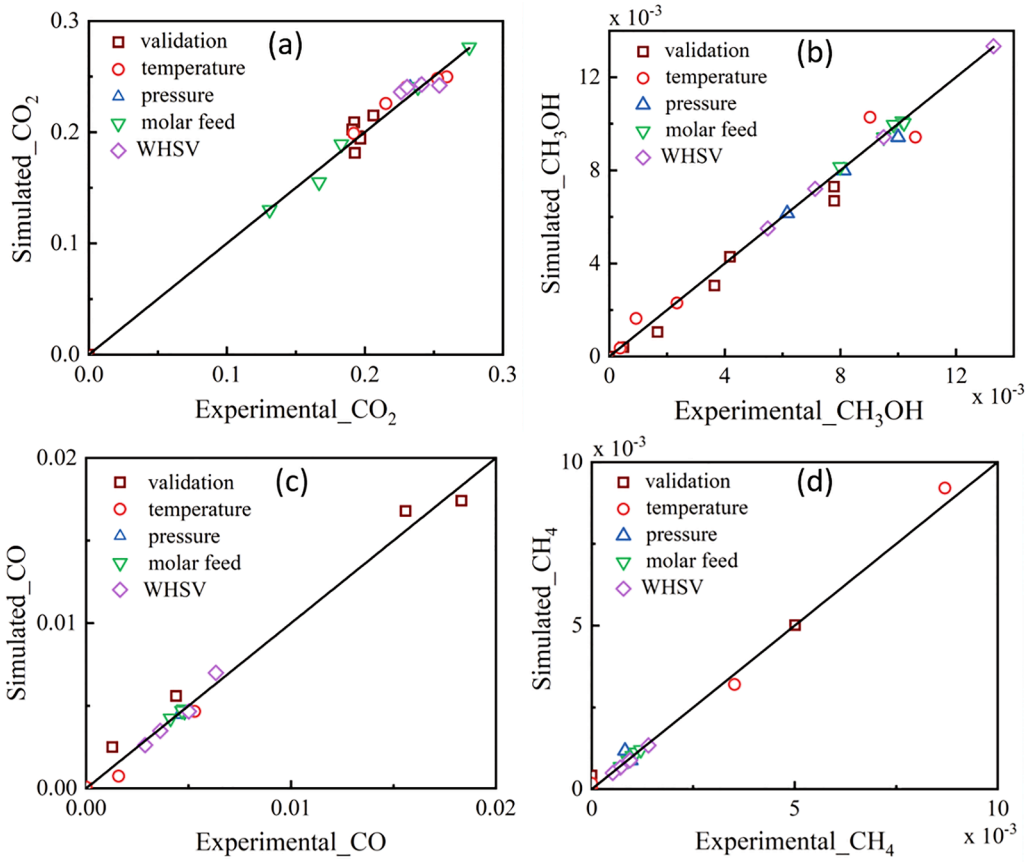

Fig. 12. Parity plots of the experimental data *vs.* the simulated single-site model results for the components (a) CO_2, (b) CH_3OH, (c) CO and (d) CH_4.

methanol steam reforming begins to occur as CO concentration increases. To establish the superiority of the single-site model, a comparison was made with a dual-site model. The developed single-site model was capable of yielding appropriate apparent orders for the reactions w.r.t. the reactant concentrations because it was better at properly predicting the experimental data with variations in molar feed ratios and total pressure as compared to the dual-site model. These results underline the importance of competitive adsorption effects on the reaction kinetics for this catalyst. Apparent activation energies of 90 and 110 kJ mol^{-1} respectively for CO_2 hydrogenation to methanol and the RWGS reactions were obtained over the In_2O_3 catalyst derived from experimental reaction rates. The parity plots showed good agreement between the experimental yields of each species and those calculated from the model. Significantly w.r.t. the CO_2 partial pressure, the reaction rates initially were found to increase and then slightly decrease indicating a varying order of the reaction. The single-site model is consistent with all the experimental data obtained from the In_2O_3 catalyst under different reaction conditions that confirm the robustness of the model. Further, this kinetic modeling study over In_2O_3 catalyst for CO_2 hydrogenation reaction should continue by investigating the influence of product components such as CO, methanol and water on the kinetics. These detailed investigations of the kinetic model for methanol synthesis over the In_2O_3 catalyst can be used for further reactor and process design.

Declaration of Competing Interest

The authors declare that they have no known competing financial interests or personal relationships that could have appeared to influence the work reported in this paper.

Acknowledgments

This work was conducted at the Chemical Engineering division and the Competence Centre for Catalysis (KCK), Chalmers University of Technology. The work is funded by the Swedish Energy Agency (47450-1 and 48387-1) and it was performed in collaboration with IVL Swedish Environmental Research Institute, Jämtkraft, Chemical Engineering at Lund University, Fly Green Fund och NISA, AFAB and The Power Region. Part of the characterization was performed in the Chalmers Materials Analysis Lab (CMAL). XPS has been performed in the Department of Industrial and Material Science, Chalmers.

Appendix A. Supplementary data

Supplementary data to this article can be found online at https://doi.org/10.1016/j.cej.2021.129120.

References

[1] H. Yang, C. Zhang, P. Gao, H. Wang, X. Li, L. Zhong, W. Wei, Y. Sun, A review of the catalytic hydrogenation of carbon dioxide into value-added hydrocarbons, Catal. Sci. Technol. 7 (20) (2017) 4580–4598.
[2] W. Wang, S. Wang, X. Ma, J. Gong, Recent advances in catalytic hydrogenation of carbon dioxide, Chem. Soc. Rev. 40 (7) (2011) 3703, https://doi.org/10.1039/c1cs15008a.
[3] M.S. Frei, M. Capdevila-Cortada, R. García-Muelas, C. Mondelli, N. López, J. A. Stewart, D. Curulla Ferré, J. Pérez-Ramírez, Mechanism and microkinetics of methanol synthesis via CO_2 hydrogenation on indium oxide, J. Catal. 361 (2018) 313–321.
[4] L.C. Grabow, M. Mavrikakis, Mechanism of methanol synthesis on cu through CO_2 and CO hydrogenation, ACS Catal. 1 (4) (2011) 365–384.
[5] A.A. Kiss, J.J. Pragt, H.J. Vos, G. Bargeman, M.T. de Groot, Novel efficient process for methanol synthesis by CO_2 hydrogenation, Chem. Eng. J. 284 (2016) 260–269.
[6] M. Huš, V.D.B.C. Dasireddy, N. Strah Štefančič, B. Likozar, Mechanism, kinetics and thermodynamics of carbon dioxide hydrogenation to methanol on $Cu/ZnAl_2O_4$ spinel-type heterogeneous catalysts, Appl. Catal. B Environ. 207 (2017) 267–278.

[7] N.M. Martin, P. Velin, M. Skoglundh, M. Bauer, P.-A. Carlsson, Catalytic hydrogenation of CO_2 to methane over supported Pd, Rh and Ni catalysts, Catal. Sci. Technol. 7 (5) (2017) 1086–1094.

[8] J.-F. Portha, K. Parkhomenko, K. Kobl, A.-C. Roger, S. Arab, J.-M. Commenge, L. Falk, Kinetics of methanol synthesis from carbon dioxide hydrogenation over copper-zinc oxide catalysts, Ind. Eng. Chem. Res. 56 (45) (2017) 13133–13145.

[9] G. Lopez, J. Alvarez, M. Amutio, B. Hooshdaran, M. Cortazar, M. Haghshenasfard, S.H. Hosseini, M. Olazar, Kinetic modeling and experimental validation of biomass fast pyrolysis in a conical spouted bed reactor, Chem. Eng. J. 373 (2019) 677–686.

[10] Q. Song, X. Wang, C. Gu, N. Wang, H. Li, H. Su, J. Huo, Y. Qiao, A comprehensive model of biomass char-CO_2 gasification reactivity with inorganic element catalysis in the kinetic control zone based on TGA analysis, Chem. Eng. J. 398 (2020), 125624.

[11] L. Yan, Y. Cao, B. He, On the kinetic modeling of biomass/coal char co-gasification with steam, Chem. Eng. J. 331 (2018) 435–442.

[12] G. Liu, D. Willcox, M. Garland, H.H. Kung, The rate of methanol production on a copper-zinc oxide catalyst: The dependence on the feed composition, J. Catal. 90 (1984) 139–146.

[13] P. Wu, B. Yang, Significance of surface formate coverage on the reaction kinetics of methanol synthesis from CO_2 hydrogenation over Cu, ACS Catal. 7 (2017) 7187–7195.

[14] F. Studt, M. Behrens, E.L. Kunkes, N. Thomas, S. Zander, A. Tarasov, J. Schumann, E. Frei, J.B. Varley, F. Abild-Pedersen, J.K. Nørskov, R. Schlögl, The mechanism of CO and CO_2 hydrogenation to methanol over Cu-based catalysts, ChemCatChem. 7 (2015) 1105–1111.

[15] X. Zhang, J.X. Liu, B. Zijlstra, I.A.W. Filot, Z. Zhou, S. Sun, E.J.M. Hensen, Optimum Cu nanoparticle catalysts for CO_2 hydrogenation towards methanol, Nano Energy. 43 (2018) 200–209.

[16] C. Huang, J. Wen, Y. Sun, M. Zhang, Y. Bao, Y. Zhang, L. Liang, M. Fu, J. Wu, D. Ye, L. Chen, CO_2 hydrogenation to methanol over Cu/ZnO plate model catalyst: Effects of reducing gas induced Cu nanoparticle morphology, Chem. Eng. J. 374 (2019) 221–230.

[17] K. Klier, V. Chatikavanij, R.G. Herman, G.W. Simmons, Catalytic synthesis of methanol from CO H_2. IV. The effects of carbon dioxide, J. Catal. 74 (1982) 343–360.

[18] P. Villa, P. Forzattl, G. Buzzl-Ferrarls, G. Garone, I. Pasquon, Synthesis of alcohols from carbon oxides and hydrogen. 1. Kinetics of the low-pressure methanol synthesis, Ind. Eng. Chem. Process Des. Dev. 24 (1985) 12–19.

[19] G.H. Graaf, E.J. Stamhuis, A.A.C.M. Beenackers, Kinetics of low-pressure methanol synthesis, Chem. Eng. Sci. 43 (1988) 3185–3195.

[20] G.H. Graaf, P.J.J.M. Sijtsema, E.J. Stamhuis, G.E.H. Joosten, Chemical equilibria in methanol synthesis, Chem. Eng. Sci. 41 (1986) 2883–2890.

[21] G.H. Graaf, H. Scholtens, E.J. Stamhuis, A.A.C.M. Beenackers, Intra-particle diffusion limitations in low-pressure methanol synthesis, Chem. Eng. Sci. 45 (1990) 773–783.

[22] R. Guil-López, N. Mota, J. Llorente, E. Millán, B. Pawelec, J.L.G. Fierro, R. M. Navarro, Methanol synthesis from CO_2: A review of the latest developments in heterogeneous catalysis, Materials. 12 (2019).

[23] T.S. Askgaard, J.K. Nørskov, C.V. Ovesen, P. Stoltze, A kinetic model of methanol synthesis, J. Catal. 156 (1995) 229–242.

[24] C.V. Ovesen, B.S. Clausen, J. Schiøtz, P. Stoltze, H. Topsøe, J.K. Nørskov, Kinetic implications of dynamical changes in catalyst morphology during methanol synthesis over Cu/ZnO catalysts, J. Catal. 168 (1997) 133–142.

[25] P.B. Rasmussen, P.M. Holmblad, T. Askgaard, C.V. Ovesen, P. Stoltze, J.K. Nørskov, I. Chorkendorff, Methanol synthesis on Cu(100) from a binary gas mixture of CO_2 and H_2, Catal. Letters. 26 (1994) 373–381.

[26] P.B. Rasmussen, M. Kazuta, I. Chorkendorff, Synthesis of methanol from a mixture of H_2 and CO_2 on Cu(100), Surf. Sci. 318 (1994) 267–280.

[27] Y. Slotboom, M.J. Bos, J. Pieper, V. Vrieswijk, B. Likozar, S.R.A. Kersten, D.W. F. Brilman, Critical assessment of steady-state kinetic models for the synthesis of methanol over an industrial Cu/ZnO/Al_2O_3 catalyst, Chem. Eng. J. 389 (2020), 124181.

[28] O. Martin, A.J. Martín, C. Mondelli, S. Mitchell, T.F. Segawa, R. Hauert, C. Drouilly, D. Curulla-Ferré, J. Pérez-Ramírez, Indium oxide as a superior catalyst for methanol synthesis by CO_2 hydrogenation, Angew. Chemie - Int. Ed. 55 (2016) 6261–6265.

[29] K. Sun, Z. Fan, J. Ye, J. Yan, Q. Ge, Y. Li, W. He, W. Yang, C.J. Liu, Hydrogenation of CO_2 to methanol over In_2O_3 catalyst, J. CO_2 Util. 12 (2015) 1–6.

[30] J. Ye, C. Liu, Q. Ge, DFT study of CO_2 adsorption and hydrogenation on the In_2O_3 surface, J. Phys. Chem. C. 116 (2012) 7817–7825.

[31] J. Ye, C. Liu, D. Mei, Q. Ge, Active oxygen vacancy site for methanol synthesis from CO_2 hydrogenation on In_2O_3 (110): A DFT study, ACS Catal. 3 (2013) 1296–1306.

[32] M.S. Frei, C. Mondelli, R. García-Muelas, K.S. Kley, B. Puértolas, N. López, O. V. Safonova, J.A. Stewart, D. Curulla Ferré, J. Pérez-Ramírez, Atomic-scale engineering of indium oxide promotion by palladium for methanol production via CO_2 hydrogenation, Nat. Commun. 10 (2019) 1–11.

[33] J. Díez-Ramírez, J.A. Díaz, F. Dorado, P. Sánchez, Kinetics of the hydrogenation of CO_2 to methanol at atmospheric pressure using a Pd-Cu-Zn/SiC catalyst, Fuel Process. Technol. 173 (2018) 173–181.

[34] D. Zhang, P. Fan, D. Wu, Y. Li, Pressure drop across a fixed bed reactor with mechanical failure of catalyst pellets described by simplified ergun's equation, China Particuology. 3 (2005) 23–25.

[35] S. Dang, B. Qin, Y. Yang, H. Wang, J. Cai, Y. Han, S. Li, P. Gao, Y. Sun, Rationally designed indium oxide catalysts for CO_2 hydrogenation to methanol with high activity and selectivity, Sci. Adv. 6 (2020) 1–11.

[36] L.B. Hoch, T.E. Wood, P.G. O'Brien, K. Liao, L.M. Reyes, C.A. Mims, G.A. Ozin, The rational design of a single-component photocatalyst for gas-phase CO_2 reduction using both UV and visible light, Adv. Sci. 1 (2014) 1400013.

[37] H. Lorenz, W. Jochum, B. Klötzer, M. Stöger-Pollach, S. Schwarz, K. Pfaller, S. Penner, Novel methanol steam reforming activity and selectivity of pure In_2O_3, Appl. Catal. A Gen. 347 (2008) 34–42.

[38] M.S. Frei, C. Mondelli, M.I.M. Short, J. Pérez-Ramírez, Methanol as a hydrogen carrier: Kinetic and thermodynamic drivers for its CO_2-based synthesis and reforming over heterogeneous catalysts, ChemSusChem. 13 (2020) 6330–6337.